APPENDIX

APPENDIX A

The Joint Committee for Powder Diffraction Standards (JCPDS)

A.1 MoO_3

Reference code:	05-0508
Mineral name:	Molybdite, syn
PDF index name:	Molybdenum Oxide
Empirical formula:	MoO_3
Chemical formula:	MoO_3

A.1.1Crystallographic parameters

Crystal system:	Orthorhombic
Space group:	Pbnm
Space group number:	62
a (˚A):	3.9620
b (˚A):	13.8580
c (˚A):	3.6970
Alpha (θ):	90.0000
Beta (θ):	90.0000
Gamma (θ):	90.0000
Calculated density:	4.71
Volume of cell:	202.99
Z:	4.00
RIR:	3.00

A.1.2 Subfiles and Quality

Subfiles:	Inorganic
	Mineral
	Alloy, metal or intermetalic
	Corrosion
	Common Phase
	Educational pattern
	Forensic
	NBS pattern
Quality:	Star (S)

A.1.3 Comments

Color:	Park gray metallic
General comments:	*Merck Index*, 8th Ed., p. 699.
	Color from *Dana's System of Mineralogy, 7th Ed.*,I 329.
Sample source:	Sample from Merck Chemical Company.
Analysis:	Spectroscopic analysis: <0.1%, Al, Co, Mn, Si; <0.01% Fe; <0.001% Cu, Mg; <0.0001% Ca.
Additional pattern:	To replace 1-706 and 5-506.
Melting point:	1185˚C
Temperature:	Pattern taken at 26 C.

A.1.4 References

Primary reference: Swanson, Fuyat.,*Natl. Bur. Stand. (U.S.), Circ. 539*, **III**, 30, (1954)

A.1.5 Peak list

No.	h	k	l	d [A]	I [%]
1	0	2	0	6.93000	34.0
2	1	1	0	3.81000	82.0
3	0	4	0	3.46300	61.0
4	0	2	1	3.26000	100.0
5	1	3	0	3.00600	13.0
6	1	0	1	2.70200	19.0
7	1	1	1	2.65500	35.0
8	1	4	0	2.60700	6.0
9	0	4	1	2.52700	12.0
10	1	3	1	2.33200	12.0
11	0	6	0	2.30900	31.0
12	1	5	0	2.27100	18.0
13	1	4	1	2.13100	9.0
14	1	6	0	1.99600	4.0
15	2	0	0	1.98200	13.0
16	2	1	0	1.96000	17.0
17	0	0	2	1.84900	21.0
18	2	3	0	1.82100	11.0
19	1	7	0	1.77100	5.0
20	1	6	1	1.75600	5.0
21	2	1	1	1.73300	17.0
22	2	2	1	1.69300	8.0
23	1	1	2	1.66300	13.0
24	0	4	2	1.63100	13.0
25	1	7	1	1.59700	15.0
26	1	8	0	1.58700	6.0
27	0	8	1	1.56900	16.0
28	2	6	0	1.50400	5.0

No.	h	k	l	d [A]	I [%]
29	2	5	1	1.47700	10.0
30	0	6	2	1.44300	12.0
31	1	9	0	1.43500	12.0
32	2	7	0	1.40000	5.0
33	0	10	0	1.38600	5.0
34	2	0	2	1.35200	6.0

A.1.6 Stick Pattern

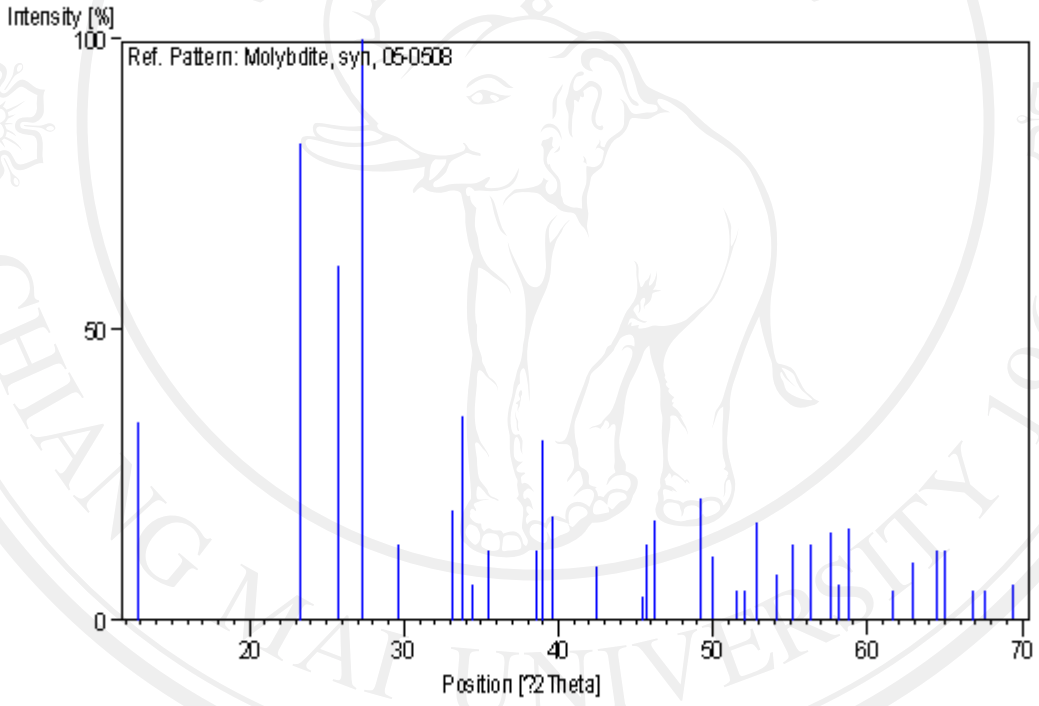

A.2 Cu

A.2.1 Name and formula

Reference code:	00-004-0836
Mineral name:	Copper, syn
PDF index name:	Copper
Empirical formula:	Cu
Chemical formula:	Cu

A.2.2 Crystallographic parameters

Crystal system:	Cubic
Space group:	Fm3m
Space group number:	225
a (˚A):	3.6150
b (˚A):	3.6150
c (˚A):	3.6150
Alpha (θ):	90.0000
Beta (θ):	90.0000
Gamma (θ):	90.0000
Calculated density (g/cm^3):	8.94
Measured density (g/cm^3):	8.95
Volume of cell (10^6 pm^3):	47.24
Z:	4.00
RIR:	-

A.2.3 Subfiles and Quality

Subfiles:	Inorganic
	Mineral
	Alloy, metal or intermetalic

Common Phase

Educational pattern

Forensic

NBS pattern

Quality: Star (S)

A.2.4 Comments

Color: Red

General comments: Impurities from 0.001-0.01%, Ag, Al, Bi, Fe, Si, Zn.Opaque mineral optical data on specimen from unspecified locality, R_3R%=60.65, Disp.=Std., VHN_{100}=96-104,Ref.:IMA Commission on Ore Microscopy QDF. Measured density and color from *Dana's System of Mineralogy, 7th Ed.*, **I** 99.

Sample source: Sample from metallurgical laboratory of NBS, Gaithersburg, MD, USA.

Sample preparation: It had been heated in an H_2 atmosphere at 300 ˚C.

Melting point: 1083˚C

Temperature: Pattern taken at 26 ˚C.

A.2.5 References

Primary reference: Swanson, Tatge.,*Natl. Bur. Stand. (U.S.), Circ. 539*, **I**, 15, (1953)

A.2.6 Peak list

No.	h	k	l	d [A]	2Theta[deg]	I [%]
1	1	1	1	2.08800	43.298	100.0
2	2	0	0	1.80800	50.434	46.0
3	2	2	0	1.27800	74.133	20.0
4	3	1	1	1.09000	89.934	17.0
5	2	2	2	1.04360	95.143	5.0
6	4	0	0	0.90380	116.923	3.0
7	3	3	1	0.82930	136.514	9.0
8	4	2	0	0.80830	144.723	8.0

A.2.7 Stick Pattern

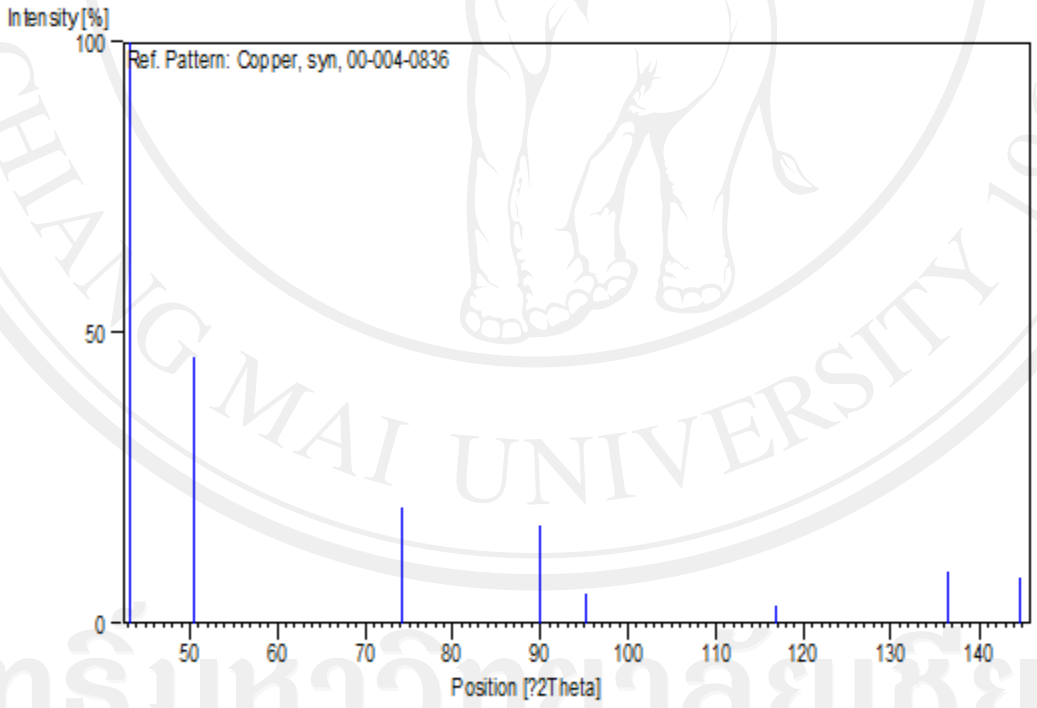

A.3 Cu_2O

A.3.1 Name and formula

Reference code:	01-078-2076
Mineral name:	Cuprite
ICSD name:	Copper Oxide
Empirical formula:	Cu_2O
Chemical formula:	Cu_2O

A.3.2 Crystallographic parameters

Crystal system:	Cubic
Space group:	Pn3m
Space group number:	224
a (˚A):	4.2670
b (˚A):	4.2670
c (˚A):	4.2670
Alpha (θ):	90.0000
Beta (θ):	90.0000
Gamma (θ):	90.0000
Calculated density (g/cm^3):	6.12
Volume of cell (10^6 pm^3):	77.69
Z:	2.00
RIR:	8.28

A.3.3 Status, subfiles and quality

Status:	Diffraction data collected at non ambient temperature
Subfiles:	Inorganic Mineral

	Alloy, metal or intermetalic
	Corrosion
	Modelled additional pattern
Quality:	Calculated (C)

A.3.4 Comments

Sample source:	Specimen from USA.
ICSD collection code:	063281

A.3.5 References

Primary reference:	*Calculated from ICSD using POWD-12++*, (1997)
Structure:	Restori, R., Schwarzenbach, D., *ActaCrystallogr., Sec. B: Structural Science*, **42**, 201, (1986)

A.3.6 Peak list

No.	h	k	l	d [A]	2Theta[deg]	I [%]
1	1	1	0	3.01723	29.583	5.3
2	1	1	1	2.46355	36.441	100.0
3	2	0	0	2.13350	42.329	34.7
4	2	1	1	1.74200	52.488	1.1
5	2	2	0	1.50861	61.408	26.5
6	2	2	1	1.42233	65.582	0.1
7	3	1	0	1.34934	69.622	0.3
8	3	1	1	1.28655	73.558	19.8
9	2	2	2	1.23178	77.417	4.3
10	3	2	1	1.14040	84.980	0.2

A.3.7 Stick Pattern

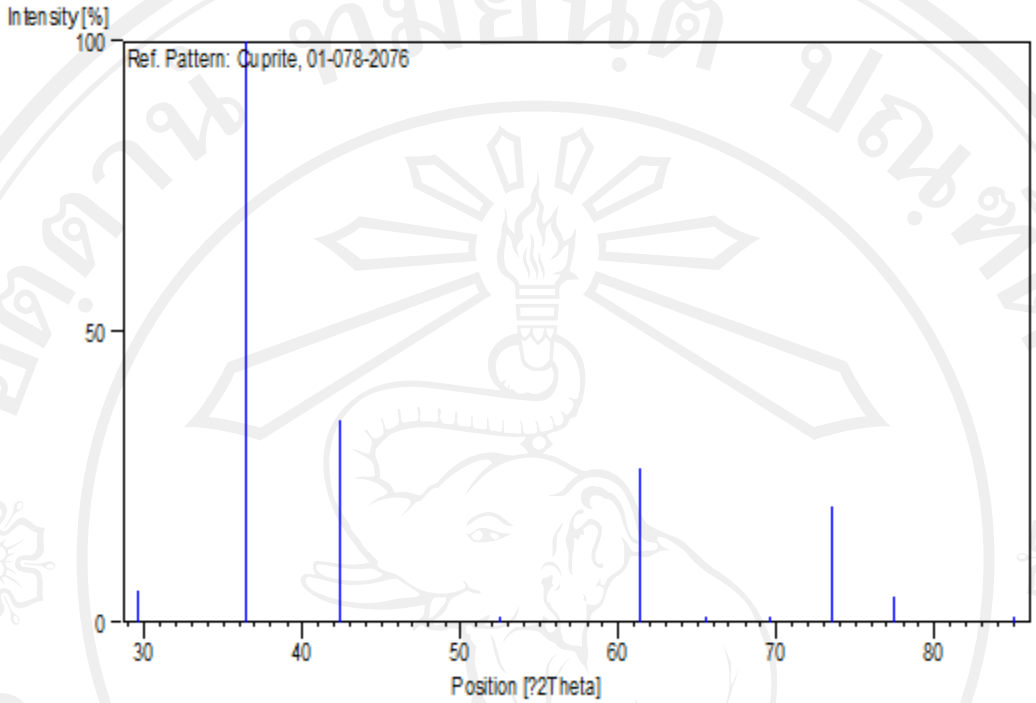

A.4 CuO

A.4.1 Name and formula

Reference code:	00-048-1548
Mineral name:	Tenorite, syn
PDF index name:	Copper Oxide
Empirical formula:	CuO
Chemical formula:	CuO

A.4.2 Crystallographic parameters

Crystal system:	Monoclinic
Space group:	C2/c
Space group number:	15
a (˚A):	4.6883
b (˚A):	3.4229
c (˚A):	5.1319
Alpha (θ):	90.0000
Beta (θ):	99.5060
Gamma (θ):	90.0000
Calculated density (g/cm^3):	6.51
Volume of cell (10^6 pm^3):	81.22
Z:	4.00
RIR:	-

A.4.3 Subfiles and Quality

Subfiles:	Inorganic
	Mineral
	Alloy, metal or intermetalic
	Corrosion

Common Phase
Forensic
Superconducting Material

Quality: Star (S)

A.4.4 Comments

Sample preparation: $Cu_2(OH)_3NO_3$ was thermally decomposed to form CuO. This was annealed at 1000 C in air for 5 hours.

Additional pattern: To replace 5-661.

A.4.5 References

Primary reference: Langford, J., Louer, D., *J. Appl. Crystallogr.*, **24**, 149, (1991)

A.4.6Peak list

No.	h	k	l	d [A]	2Theta[deg]	I [%]
1	1	1	0	2.75201	32.509	13.0
2	0	0	2	2.53236	35.418	37.0
3	1	1	-1	2.52367	35.544	100.0
4	1	1	1	2.32429	38.709	99.0
5	2	0	0	2.31315	38.903	21.0
6	1	1	-2	1.96095	46.260	3.0
7	2	0	-2	1.86764	48.717	30.0
8	1	1	2	1.77808	51.344	1.0
9	0	2	0	1.71179	53.487	7.0
10	0	2	1	1.62105	56.743	1.0
11	2	0	2	1.58227	58.265	10.0
12	1	1	-3	1.50600	61.526	20.0

No.	h	k	l	d [A]	2Theta[deg]	I [%]
13	0	2	2	1.41789	65.813	10.0
14	3	1	-1	1.41013	66.222	15.0
15	3	1	0	1.40586	66.449	1.0
16	1	1	3	1.37922	67.905	6.0
17	2	2	0	1.37530	68.125	14.0
18	2	2	-1	1.36158	68.907	1.0
19	3	1	-2	1.31552	71.683	1.0
20	3	1	1	1.30467	72.373	5.0
21	2	2	1	1.29586	72.944	1.0
22	0	0	4	1.26567	74.978	6.0
23	2	2	-2	1.26184	75.245	5.0
24	0	2	3	1.20171	79.733	1.0
25	2	0	-4	1.19642	80.157	2.0
26	1	1	-4	1.19538	80.241	1.0
27	3	1	-3	1.16989	82.362	4.0
28	2	2	2	1.16176	83.065	2.0
29	3	1	2	1.15604	83.568	2.0
30	4	0	-2	1.12388	86.533	1.0
31	2	2	-3	1.12137	86.775	1.0
32	1	1	4	1.10921	87.968	1.0
33	1	3	0	1.10835	88.054	1.0
34	1	3	-1	1.09137	89.790	3.0
35	1	3	1	1.07330	91.729	1.0
36	2	0	4	1.04010	95.565	1.0
37	2	2	3	1.01764	98.392	1.0
38	3	1	3	1.00789	99.684	2.0
39	4	0	2	0.99164	101.935	1.0
40	1	1	-5	0.98184	103.357	2.0
41	2	2	-4	0.98044	103.565	2.0
42	4	2	0	0.95795	107.049	2.0

No.	h	k	l	d [A]	2Theta[deg]	I [%]
43	1	3	-3	0.94314	109.519	1.0
44	4	2	-2	0.93939	110.170	3.0
45	4	0	-4	0.93362	111.191	1.0
46	1	1	5	0.92115	113.489	2.0
47	4	2	1	0.91816	114.060	1.0
48	1	3	3	0.90959	115.744	1.0
49	5	1	-1	0.90421	116.838	1.0
50	2	2	4	0.88848	120.221	1.0
51	3	3	1	0.88720	120.509	3.0

A.4.7 Stick Pattern

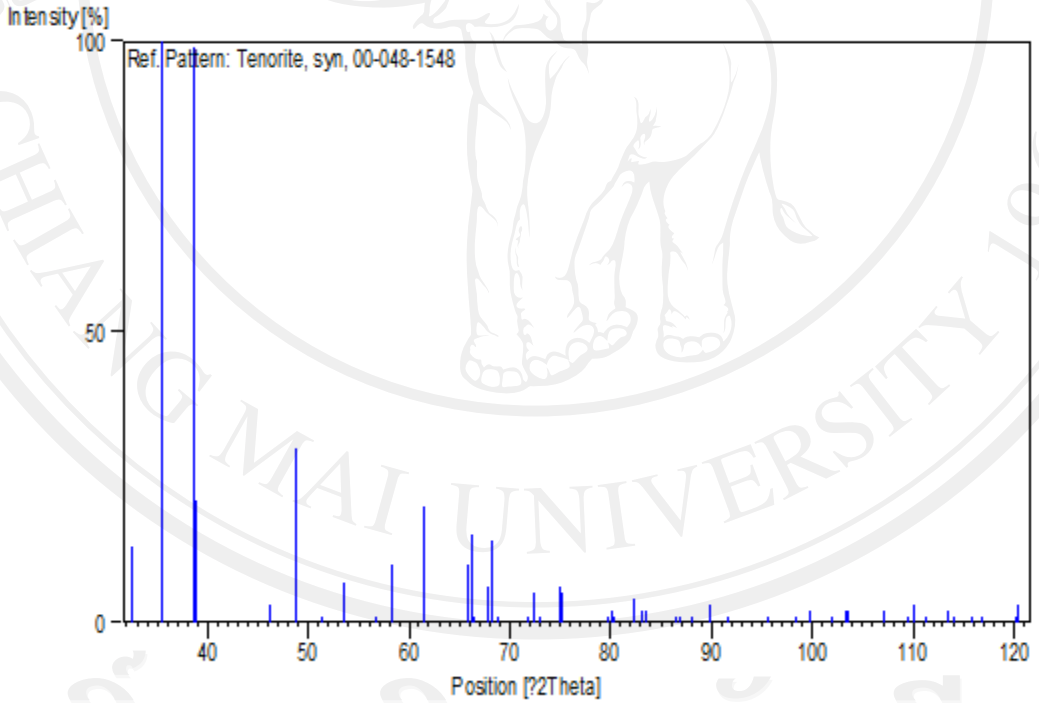

APPENDIX B

Camera constant used for the indexing of SAED pattern

Table B.1 Camera constant (Lλ) at 200 kV of JEOL-TEM

L (cm)	D111Au (mm)	r111Au (mm)	D111Auv(A)	Lλ(mm.A)
40	8.70	4.35	2.355	10.2442
60	13.2	6.60	2.355	15.5430
80	17.2	8.60	2.355	20.2530
100	21.2	10.60	2.355	24.963
120	25.2	12.60	2.355	29.6730
150	31.5	15.75	2.355	37.0912
200	41.5	20.75	2.355	48.8662
250	51.8	25.90	2.355	60.9945

APPENDIX C

NH_3 gas flow rate controller (Cole-Parmer model PMR 1-010333)

Table B.2 NH_3 gas flow rate controlled by gas regulator (Cole-Parmer model PMR 1-010333)

Feeding time (s)	Flowing volume at scale (cm^3)	
	5	**10**
1	2.114	2.445
2	4.228	4.890
3	6.342	7.335
4	8.456	9.780
5	10.570	12.225
6	12.684	14.670
7	14.798	17.115
8	16.912	19.560
9	19.026	22.005
10	21.140	24.450
11	23.254	26.895
12	25.368	29.340
13	27.482	31.785
14	29.596	34.230
15	31.710	36.675

CURRICULUM VITAE

Author's Name Mr. Arrak Klinbumrung

Date of birth October 21, 1980

Place of Birth Chainat, Thailand

Education

2002	B.S. (Physics), Naresuan University, Thailand
2005	M.Sc. (Materials Science), Chiang Mai University, Thailand
2014	Ph.D. (Materials Science), Chiang Mai University, Thailand

Scholarships

2010-2013	Thailand's Office of the Higher Education Commission through the program of the Higher Education Research Promotion (HERP)
2013	Financial support for graduate student research, Graduated School, Chiang Mai University

Publications

(1) Arrak Klinbumrung, Titipun Thongtem and Somchai Thongtem, Characterization of Orthorhombic α-MoO_3 Microplates Produced by a Microwave Plasma Process, Journal of Nanomaterials, 2012 (2012) Article ID: 930763, 5 pages.

(2) Arrak Klinbumrung, Titipun Thongtem and Somchai Thongtem Characterization and gas sensing properties of CuO synthesized by DC

directly applying voltage, Applied Surface Science, (2014), In press, http://dx.doi.org/10.1016/j.apsusc.2014.06.037

International conferences

1. Poster presentation, A. Klinbumrung, T. Thongtem and S. Thongtem**,** "Morphology Evolution of Nanostructured MoO_3 Synthesized by Microwave Plasma Process for Different Length of Time**"** was presented at The 2nd International Symposium on Hybrid Materials and Processing (HyMap 2011), October 27-29, 2011, Busan, Korea

2. Poster presentation, A. Klinbumrung, T. Thongtem and S. Thongtem**,** "Phase Characterization and Optical Properties of Orthorhombic Molybdenum Oxide Nanostructured Synthesized by Microwave Plasma Radiation" was presented at The 6th Pure and Applied Chemistry International Conference (PACCON 2012), January 11-13, 2012, Chiang Mai, Thailand

INTERNATIONAL PUBLICATIONS

Hindawi Publishing Corporation
Journal of Nanomaterials
Volume 2012, Article ID 930763, 5 pages
doi:10.1155/2012/930763

Research Article

Characterization of Orthorhombic α-MoO_3 Microplates Produced by a Microwave Plasma Process

Arrak Klinbumrung,[1] Titipun Thongtem,[2,3] and Somchai Thongtem[1,3]

[1] *Department of Physics and Materials Science, Faculty of Science, Chiang Mai University, Chiang Mai 50200, Thailand*
[2] *Department of Chemistry, Faculty of Science, Chiang Mai University, Chiang Mai 50200, Thailand*
[3] *Materials Science Research Center, Faculty of Science, Chiang Mai University, Chiang Mai 50200, Thailand*

Correspondence should be addressed to Somchai Thongtem, schthongtem@yahoo.com

Received 1 October 2011; Accepted 8 November 2011

Academic Editor: William W. Yu

Orthorhombic α-MoO_3 microplates were produced from $(NH_4)_6Mo_7O_{24}\cdot 4H_2O$ solid powder by a 900 W microwave plasma for 40, 50, and 60 min. Phase, morphologies, and vibration modes were characterized by X-ray diffraction (XRD), selected area electron diffraction (SAED), scanning electron microscopy (SEM), and Raman and Fourier transform infrared (FTIR) spectroscopy. Sixty min processing resulted in the best crystallization of the α-MoO_3 phase, with photoluminescence (PL) in a wavelength range of 430–440 nm.

1. Introduction

Basically, molybdenum oxides are classified into two types: the thermodynamically stable orthorhombic α-MoO_3 phase, and the metastable monoclinic β-MoO_3 phase with ReO_3-type structure. Orthorhombic α-MoO_3 phase is a promising oxide, with structural anisotropy [1]. It is a wide bandgap n-type semiconductor, which is very attractive for different technological applications such as photochromic materials (changing from colorless to blue by UV irradiation) [2–4], smart windows [5], self-developing photography [2], conductive gas sensors [3], lubricants [6], and catalysts [7]. Orthorhombic α-MoO_3 was composed of MoO_6 octahedral corner-sharing chains, with edge sharing of two similar chains to form layers bonded by the weak van der Waals attraction [2]. Different methods were used to produce the oxide, which led to achieving products with different properties: evaporation of Mo foil by IR in 1 atm synthetic air to produce a uniformly semitransparent film on alumina substrate [3], direct oxidation of a Mo spiral coil in ambient atmosphere to produce film on Si (001) substrate [8], flash evaporation of molybdenum oxide powder on silica glass substrate, and (111)-oriented silicon wafer in vacuum [9], precipitation [10], and hydrothermal method [11].

In the present research, α-MoO_3 microplates were produced by exposing a solid powder to microwave plasma. This very simple and rapid process, which is also benign to the environment, may lead to large-scale industrial production.

2. Experiment

To produce MoO_3, $(NH_4)_6Mo_7O_{24}\cdot 4H_2O$ powder was used as a starting material without further purification. Each 0.5 g powder was loaded into three 14 mm I.D. × 100 mm long silica boats. Each was placed in a horizontal quart tube, which was tightly closed and evacuated until its absolute pressure was 3.7 ± 0.1 kPa. The powder was heated in batches by a 900 W microwave plasma; each batch was irradiated for 5 min. After the processing of each batch, the powder was thoroughly mixed and repeatedly heated for a total of 40, 50, or 60 min. During processing, the horizontal quart tube was continuously evacuated to drain the evolved gases out of the system.

The products were characterized using X-ray diffractometer (XRD, SIEMENS D500) operating at 20 kV, 15 mA, and

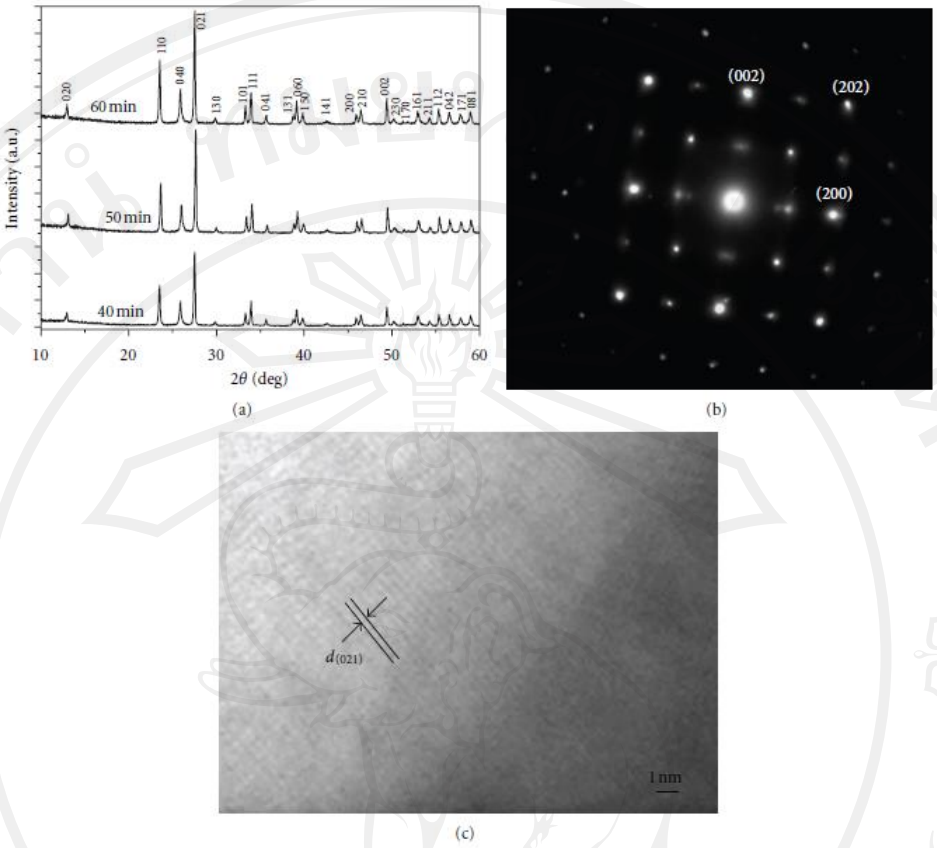

FIGURE 1: (a) XRD patterns of α-MoO_3 processed for 40, 50, and 60 min. (b, c) SAED pattern and HRTEM image of α-MoO_3 processed for 60 min.

using Cu-K_α line, in combination with the database of the Joint Committee on Powder Diffraction Standards (JCPDS) [12]; scanning electron microscope (SEM, JEOL JSM-6335F) operating at 15 kV, transmission electron microscope (TEM, JEOL JEM-2010), and selected area electron diffractometer (SAED) operating at 200 kV; Fourier transform infrared spectrometer (FTIR, Bruker Tensor 27) with KBr as a diluting agent and operated in the range of 2000–400 cm^{-1}, Raman spectrometer (T64000 HORIBA Jobin Yvon) using a 50 mW and 514.5 nm wavelength Ar green laser, and photoluminescence (PL) spectrometer (LS 50B PerkinElmer) using a 380 nm excitation wavelength at room temperature.

3. Results and Discussion

3.1. XRD, SAED, and HRTEM. XRD patterns of the products processed for 40, 50, and 60 min are shown in Figure 1(a). Their peaks were specified as orthorhombic MoO_3 of JCPDS database number 05–0508 [12], with no impurity detection. The (020) peaks at 2θ of 12.8° were clearly detected, and they indicated the presence of orthorhombic phase instead of monoclinic [13]. It should be noted that their intensities were slightly increased with the increase of processing time. The XRD peaks for 60 min processing time were the strongest, reflecting the product with the best degree of crystallinity. During processing, $(NH_4)_6Mo_7O_{24}\cdot 4H_2O$ decomposed as follows:

$$(NH_4)_6Mo_7O_{24}\cdot 4H_2O(s) \longrightarrow 7MoO_3(s) + 6NH_3(g) + 7H_2O(g) \quad (1)$$

$MoO_3(s)$ was left as the final solid products. Two gases (NH_3 and H_2O) diffused out of the system, and evacuated out of the horizontal quart tube. It should be noted that some reactant could remain, and was mixed with the final product if the processing time was less than 40 min. Longer processing times resulted in greater purification of the final product.

Calculated lattice parameters (Å) using the plane spacing equation for orthorhombic phase [14] were a = 3.96,

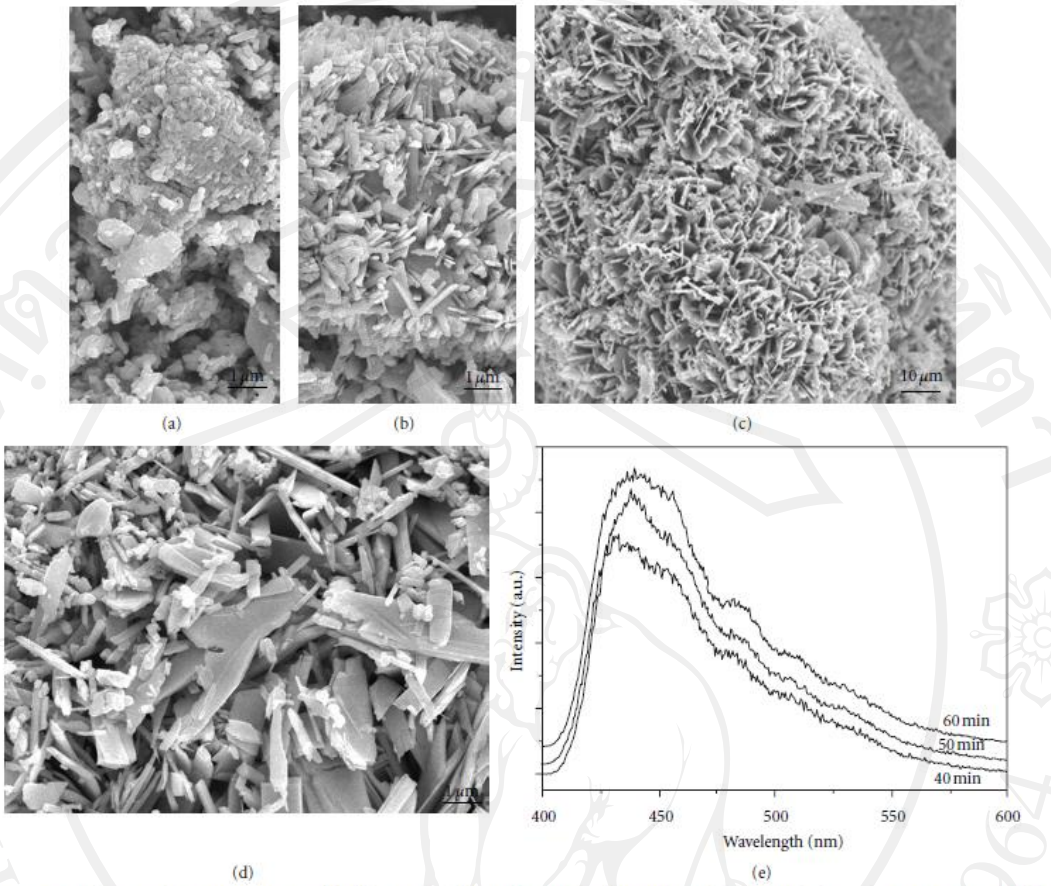

FIGURE 2: SEM images of α-MoO_3 processed for (a) 40 min, (b) 50 min, and (c, d) 60 min, and (e) PL emissions of α-MoO_3 processed for 40, 50, and 60 min.

b = 13.86, and c = 3.70, in accordance with those of the JCPDS database [12]. Figure 1(b) shows the SAED pattern of a single crystal processed for 60 min. It was indexed [15] to correspond with the (002), (202), and (200) crystallographic planes, which were specified as orthorhombic α-MoO_3 [2, 12, 16]. In the present analysis, an electron beam was sent to the crystal along the [010] direction. The (021) crystallographic plane with 0.33 nm spacing was detected by HRTEM (Figure 1(c)), implying that the product was crystalline in nature. These last two analyses were in accordance with that of the above XRD.

3.2. SEM. SEM images of MoO_3 crystals processed for 40, 50, and 60 min are shown in Figures 2(a)–2(d). Clusters of spheres ranging from 100 nm to a few hundred nm, as well as a small fraction of plates, were produced by 40 min processing. When the processing time was 50 min, more plates—about 100 nm thick and a few μm long—were produced, growing perpendicular to the cluster surface. Sixty min processing resulted in a further increase in the number of plates produced, as well as their sizes: 100–200 nm thick and a few μm long. During processing, some plates could be broken due to the internal stress developed inside.

3.3. Raman and FTIR Analyses. Raman spectra (Figure 3(a)) of MoO_3 crystals processed for 40, 50 and 60 min were studied in the range of 150–1050 cm^{-1}. During the analysis, a low-intensity laser was used to avoid crystallization. The product of 60 min processing was a highly ordered crystalline structure, and its Raman peaks were the highest. The heights were reduced when the processing time was shortened. In the present research, 12 typical Raman peaks were detected. The peaks at 990 cm^{-1} were specified as the Mo=O asymmetric stretching modes of terminal (unshared) oxygen [16]. The strongest peaks were at 813 cm^{-1}, and were specified as the doubly connected bridge-oxygen Mo_2–O stretching modes

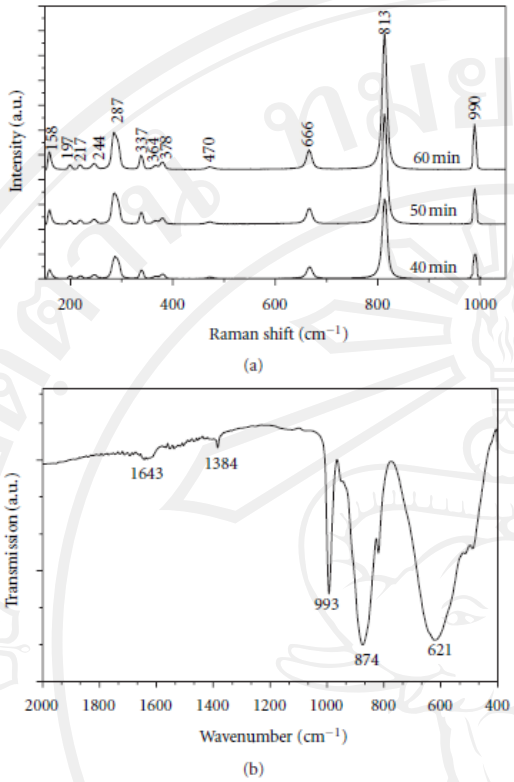

FIGURE 3: (a) Raman analysis of α-MoO_3 processed for 40, 50, and 60 min. (b) FTIR spectrum of α-MoO_3 processed for 60 min.

[2] of doubly coordinated oxygen, caused by corner-shared oxygen atoms in common to two MoO_6 octahedrons [16]. The peaks at 666 cm^{-1} were the Mo_3–O stretching modes of triply coordinated bridge-oxygen, caused by edge-shared oxygen atoms in common to three octahedrons [2, 16]. Their remains were the O–Mo–O asymmetric stretching/bending modes at 470 cm^{-1}, O–Mo–O scissoring modes at 378 and 364 cm^{-1}, O–Mo–O bending modes at 337 cm^{-1}, O=Mo=O wagging modes at 287 cm^{-1}, O=Mo=O twisting modes at 244 cm^{-1}, R_c modes at 217 cm^{-1}, O=Mo=O twisting modes at 197 cm^{-1}, and T_b modes at 158 cm^{-1} [16]. Sometimes the Raman peaks were positively/negatively shifted, due to the increase or decrease in the vibration constant of the products [2]. In the present research, the vibrations were the same values, although the processing time and degree of crystallinity were different.

Figure 3(b) shows the FTIR spectrum of α-MoO_3 over the 400–2000 cm^{-1} range. Three strong vibrations were detected at 621, 874 and 993 cm^{-1}, associated respectively with the stretching mode of oxygen linked with three metal atoms, the stretching mode of oxygen in the Mo–O–Mo units, and the Mo=O stretching mode—the specification of a layered orthorhombic α-MoO_3 phase [17]. Two weak vibrations were also detected at 1384 and 1643 cm^{-1}, associated with the vibration mode of the Mo–OH bond and the bending mode of adsorbed water, respectively [17, 18].

3.4. PL Emission. PL emission of orthorhombic α-MoO_3 processed for 40, 50, and 60 min was studied using 380 nm excitation wavelength at room temperature. The PL spectra (Figure 2(e)) presented broad peaks over the 400–600 nm range with a strong indigo emission centered at 430–440 nm—in accordance with the report of Song et al. [4]. These emissions were caused by the band-to-band transition. In the present research, very weak shoulders, caused by the electron-hole recombination between the conduction band and the sublevel of adsorbed oxygen acceptors, were also detected; these were able to be reduced by calcination at high temperatures [4]. The luminescence intensity increased with the increase of processing times, in accordance with the improvement of the degree of crystallinity characterized by the above XRD analysis.

4. Conclusions

Orthorhombic α-MoO_3 was successfully produced by a 900 W microwave plasma process for 40, 50, and 60 min. The product processed for 60 min was α-MoO_3 microplates with three main Raman peaks (666, 813, and 990 cm^{-1}), three main FTIR vibration modes (621, 874, and 993 cm^{-1}), and 430–440 nm indigo emission—a promising material for different applications.

Acknowledgments

The authors wish to thank the National Nanotechnology Center (NANOTEC), National Science and Technology Development Agency, Thailand, for providing financial support through the project code: P-10-11345, the Thailand's Office of the Higher Education Commission through the National Research University Project, and the Scholarships for Thai Ph.D. Program, and the Thailand Research Fund (TRF) through the TRF Research Grant, including the Graduate School of Chiang Mai University through the general support.

References

[1] X. W. Lou and H. C. Zeng, "Hydrothermal synthesis of α-MoO_3 nanorods via acidification of ammonium heptamolybdate tetrahydrate," *Chemistry of Materials*, vol. 14, no. 11, pp. 4781–4789, 2002.

[2] T. He and J. Yao, "Photochromism of molybdenum oxide," *Journal of Photochemistry and Photobiology C*, vol. 4, no. 2, pp. 125–143, 2003.

[3] E. Comini, L. Yubao, Y. Brando, and G. Sberveglieri, "Gas sensing properties of MoO_3 nanorods to CO and CH_3OH," *Chemical Physics Letters*, vol. 407, no. 4–6, pp. 368–371, 2005.

[4] J. Song, X. Ni, D. Zhang, and H. Zheng, "Fabrication and photoluminescence properties of hexagonal MoO_3 rods," *Solid State Sciences*, vol. 8, no. 10, pp. 1164–1167, 2006.

[5] T. He, Y. Ma, Y. Cao, Y. Yin, W. Yang, and J. Yao, "Enhanced visible-light coloration and its mechanism of MoO_3 thin films by Au nanoparticles," *Applied Surface Science*, vol. 180, no. 3-4, pp. 336–340, 2001.

[6] J. Wang, K. C. Rose, and C. M. Lieber, "Load-independent friction: MoO_3 nanocrystal lubricants," *The Journal of Physical Chemistry B*, vol. 103, no. 40, pp. 8405–8409, 1999.

[7] K. R. Reddy, K. Ramesh, K. K. Seela, V. V. Rao, and K. V. R. Chary, "Alkylation of phenol with methanol over molybdenum oxide supported on NaY zeolite," *Catalysis Communications*, vol. 4, no. 3, pp. 112–117, 2003.

[8] Y. Zhao, J. Liu, Y. Zhou et al., "Preparation of MoO_3 nanostructures and their optical properties," *Journal of Physics: Condensed Matter*, vol. 15, no. 35, pp. L547–L552, 2003.

[9] C. Julien, A. Khelfa, O. M. Hussain, and G. A. Nazri, "Synthesis and characterization of flash-evaporated MoO_3 thin films," *Journal of Crystal Growth*, vol. 156, no. 3, pp. 235–244, 1995.

[10] H. X. Bai, X. H. Liu, and Y. C. Zhang, "Synthesis of MoO_3 nanoplates from a metallorganic molecular precursor," *Materials Letters*, vol. 63, no. 1, pp. 100–102, 2009.

[11] T. Xia, Q. Li, X. Liu, J. Meng, and X. Cao, "Morphology-controllable synthesis and characterization of single-crystal molybdenum trioxide," *The Journal of Physical Chemistry B*, vol. 110, no. 5, pp. 2006–2012, 2006.

[12] Powder Diffract, File, JCPDS-ICDD, 12 Campus Boulevard, Newtown Square, P.A. 19073-3273, USA, 2001.

[13] T. Mizushima, K. Fukushima, H. Ohkita, and N. Kakuta, "Synthesis of β-MoO_3 through evaporation of HNO_3-added molybdic acid solution and its catalytic performance in partial oxidation of methanol," *Applied Catalysis A*, vol. 326, no. 1, pp. 106–112, 2007.

[14] C. Suryanarayana and M. G. Norton, *X-Ray Diffract*, Plenum Press, New York, USA, 1998.

[15] K. W. Andrews, D. J. Dyson, and S. R. Keown, *Interpretation of Electron Diffraction Patterns*, Plenum Press, New York, USA, 1971.

[16] T. Siciliano, A. Tepore, E. Filippo, G. Micocci, and M. Tepore, "Characteristics of molybdenum trioxide nanobelts prepared by thermal evaporation technique," *Materials Chemistry and Physics*, vol. 114, no. 2-3, pp. 687–691, 2009.

[17] G. S. Zakharova, C. Täschner, V. L. Volkov et al., "$MoO_{3-\delta}$ nanorods: synthesis, characterization and magnetic properties," *Solid State Sciences*, vol. 9, no. 11, pp. 1028–1032, 2007.

[18] M. Dhanasankar, K. K. Purushothaman, and G. Muralidharan, "Effect of temperature of annealing on optical, structural and electrochromic properties of sol-gel dip coated molybdenum oxide films," *Applied Surface Science*, vol. 257, no. 6, pp. 2074–2079, 2011.

G Model
APSUSC-28086; No. of Pages7
ARTICLE IN PRESS

Applied Surface Science xxx (2014) xxx–xxx

Contents lists available at ScienceDirect

Applied Surface Science

journal homepage: www.elsevier.com/locate/apsusc

Characterization and gas sensing properties of CuO synthesized by DC directly applying voltage

Arrak Klinbumrung[a], Titipun Thongtem[b,c], Somchai Thongtem[a,c,*]

[a] Department of Physics and Materials Science, Faculty of Science, Chiang Mai University, Chiang Mai 50200, Thailand
[b] Department of Chemistry, Faculty of Science, Chiang Mai University, Chiang Mai 50200, Thailand
[c] Materials Science Research Center, Faculty of Science, Chiang Mai University, Chiang Mai 50200, Thailand

ARTICLE INFO

Article history:
Received 27 February 2014
Received in revised form 4 June 2014
Accepted 6 June 2014
Available online xxx

Keywords:
CuO
Directly applying voltage
Gas sensors
Optical properties

ABSTRACT

CuO microstructure was successfully synthesized by 50 A and 3.6 V DC directly applying voltage. Crystalline structure was characterized by X-ray diffraction (XRD), morphology by scanning and transmission electron microscopy (SEM, TEM). The sample of the 15 min processing time has an irregular shape with diameter about several hundreds of nanometer. Fourier transform infrared (FTIR) spectroscopy, ultraviolet–visible (UV–vis) absorption spectroscopy and photoluminescence (PL) were used to determine vibrational modes and optical properties of the as-synthesized samples: 529 and 585 cm^{-1} vibrational modes, 3.95 eV band gap, and 402 nm emitting wavelength in violet region of CuO. X-ray photoelectron (XPS) spectroscopy was used to determine chemical composition, Cu(II)O, of the metal oxide surface. Gas sensing performance exposing to NH_3 mixed with air at various working temperatures and NH_3 concentrations of the as-synthesized CuO has the best response at the optimal working temperature of 250 °C: sensitivity of 56.6% exposed to 5275 ppm NH_3.

1. Introduction

Metal oxide (MO) semiconductors have become promising gas sensing devices due to their low cost, short responding time, long life and wide range target gas selectivity [1]. Thus, the MO gas sensors are widely studied in order to improve their sensing performance for detecting and controlling toxic gases. Among them, CuO, ZnO, SnO_2, AgO, NiO and Fe_2O_3 are the interesting MO semiconductors.

Cupric oxide (CuO), a p-type semiconductor, has attracted attention as a functional material for gas sensing application. This material has various advantages [2]: nontoxic properties, low synthetic cost and its energy gap lies in the range of solar radiation. Thus, the effort has been made to study on how to synthesize the oxide. There have been a number of methods used for the synthesis of CuO with different morphologies, such as direct oxidation [3], microwave-hydrothermal process without adding any surfactants [4], chemical route [5] and alcothermal method [6].

In this research, CuO microstructures were synthesized by DC directly applying voltage under different length of processing time. This process is fast, simple and effective. Phase, structure, optical properties and gas sensing performance were investigated and discussed.

2. Experiment

Our experiment was carried out by a lab-made DC directly applying voltage (Fig. 1). Copper powder (99%, Fluka & Riedel-de Haën) was placed between the 2 cm diameter stainless steel electrodes which were connected with DC power supply (Welpro, Welarc 200). To produce copper oxide, the powder was heated by DC electrical supply which directly applied electrical current (50 A, 3.6 V) through the powder for 1, 3, 6, 9, 12 and 15 min in ambient environment. For processing time of longer than 3 min, the powder was heated in batches for 3 min each, left cool down to room temperature, thoroughly mixed at room temperature, and repeatedly heated until reaching the complete processing time. Structural and morphological studies were performed by scanning electron microscopy (SEM, JEOL model JSM-6335F) operating at 20 kV and transmission electron microscopy (TEM, JEOL JEM-2010) operating at 200 kV. X-ray diffraction patterns of the samples were recorded on a Rigaku MiniFlex X-ray diffractometer with Cu-K_α radiation (λ = 1.54178 Å). The 2θ range used in this measurement was from

* Corresponding author at: Chiang Mai University, Department of Physics and Materials Science, Faculty of Science, 239 Huay Kaew Rd., Suthep, Chiang Mai 50200, Thailand. Tel.: +66 53941924; fax: +66 53943445.
E-mail addresses: schthongtem@yahoo.com, thongtem.sch@gmail.com (S. Thongtem).

http://dx.doi.org/10.1016/j.apsusc.2014.06.037
0169-4332/

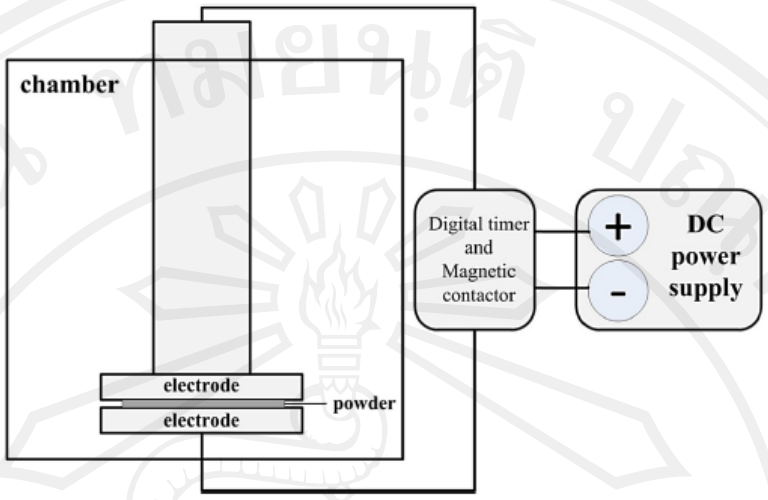

Fig. 1. Schematic diagram of a lab-made DC directly applying voltage apparatus.

30° to 80° in step of 0.02°. The optical properties were characterized using UV–vis–NIR double beam spectrophotometer (Perkin Elmer, Varian Cary 5000) in the spectral range 200 and 800 nm and photoluminescence (PL) spectrometer (Perkin Elmer, LS50B) with a 325 nm excitation wavelength at room temperature. Fourier transform infrared (FTIR) spectra were recorded on a BRUKER TENSOR 27 Fourier transform infrared spectrometer with KBr as a diluting agent and operated in the range of 400–4000 cm^{-1}. X-ray photoelectron spectroscopy (XPS) model AXIS ULTRA DLD was used to characterize chemical composition of metal oxide surface.

To fabricate a CuO gas sensing device, silver paste was painted on alumina substrates with an interval of 1 mm for using as electrodes, which were solidified by annealing the silver paste at 100 °C for 1 h. The 15 min as-synthesized CuO and DI water were mixed to formulate paste which was used to synthesize films by screen printing. The films were dried at 150 °C for 2 h to remove the binder and to improve the mechanical strength and electrical contact. The measurement of gas sensing properties was studied through a simple static system under normal laboratory condition. The tested gas (NH_3) was calculated the volume before injecting into the air-trapped chamber for controlling the gas concentration. The resistance of sensor was obtained through the electrical current change between those before and after injecting the tested gas to the system (Fig. 2). The sensitivity (S) can be calculated according to the relation

$$S(\%) = \frac{I_{air} - I_{gas}}{I_{air}} \times 100, \quad (1)$$

where I_{air} and I_{gas} are the electrical current of the sensor in the surrounding air and tested gas mixture at the same temperature, respectively.

3. Results and discussion

The XRD patterns of the 50 A and 3.6 V as-synthesized powder at different length of processing time are shown in Fig. 3. According to the JCPDS database, all diffraction peaks can be indexed as follows. For 1 min processing time, the solid mixture of cubic Cu (JCPDS No 004-0836) and cubic Cu_2O (JCPDS No 078-2076) were detected. Monoclinic CuO (JCPDS No 048-1548) was revealed as a component of mixture at 3 min heating time. Cu peaks became a

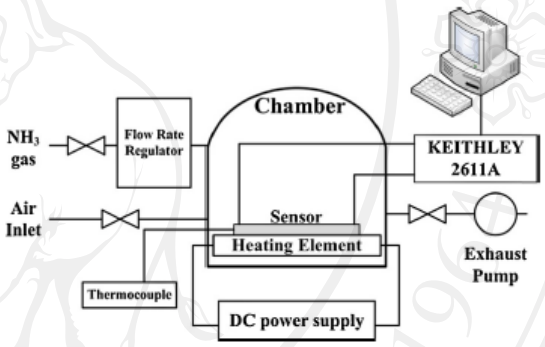

Fig. 2. Schematic diagram of a lab-made gas sensing measurement system.

small fraction at 6 min and were no longer detected when the processing time was reach 9 min. At 12 min processing time, Cu_2O still contains as an impurity of CuO main phase. For the 15 min processing time, crystalline CuO was successfully synthesized without any impurity detection. During processing, oxygen gradually diffused into Cu matrix and formed Cu_2O as a primary metal oxide. Then the Cu_2O crystal transformed into CuO, described by the following equation: $2Cu_2O + O_2 \rightarrow 4CuO$ [8]. The prolonged time of batch processing was able to enrich oxygen to further oxidize Cu^{1+} to Cu^{2+}. The conversion of Cu_2O to CuO at the temperature above 400 °C was reported [9].

The lattice constants of CuO pure phase were calculated using the least square refinement from the UNITCELL-97 program [7]. The calculated lattice parameters (a = 4.6922 Å, b = 3.4253 Å and c = 5.1340 Å with β = 99.4575°) are in accordance with those of the JCPDS No 048-1548 with lattice constants of a = 4.6883 Å, b = 3.4229 Å, c = 5.1319 Å, and β = 99.5060°.

The average size of crystallite (G_{hkl}) was estimated by the classical Scherrer's formula

$$G_{hkl} = \frac{0.9\lambda}{D \cos\theta}, \quad (2)$$

Please cite this article in press as: A. Klinbumrung, et al., Characterization and gas sensing properties of CuO synthesized by DC directly applying voltage, Appl. Surf. Sci. (2014), http://dx.doi.org/10.1016/j.apsusc.2014.06.037

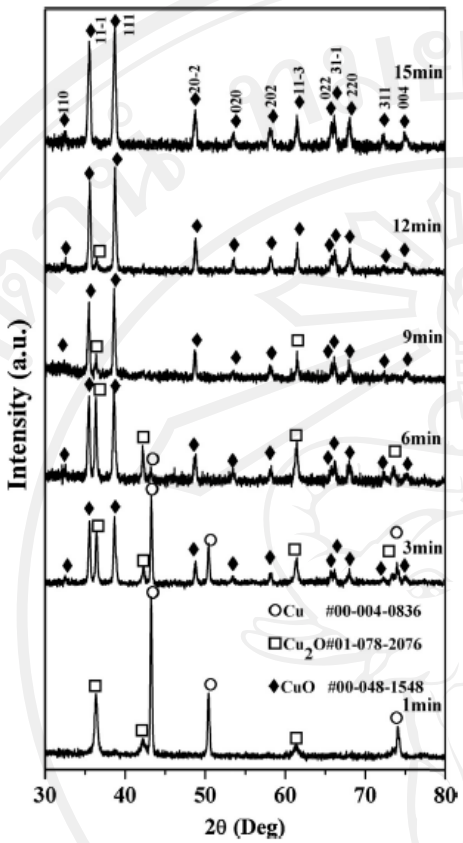

Fig. 3. XRD patterns of the samples synthesized for 1, 3, 6, 9, 12 and 15 min processing times.

where λ is the wavelength of the incident X-ray (Cu-K_α radiation source with 0.15418 nm), D is the full width at half maximum (FWHM) and θ is the Bragg's angle. The (1 1 1) strongest peak was used for calculation. The crystallite size for 15 min heating time is 143 nm.

In this research, the as-synthesized samples were studied without any further processing. TEM image of the 15 min processing time is shown in Fig. 4a. The particle has an irregular shape with 433 nm in length and 305 nm in width. Crystalline structure of 15 min processing time was also simulated by VESTA version 3.0 program (Fig. 4b). The morphology of the samples was examined by SEM. Fig. 5 shows typical SEM images of the as-synthesized samples composing of agglomerated particles with irregular shape. For 1 min long, Cu particles melt to form as necking of the surrounding particles. Initially, particles have an average diameter of 2.75 μm. Oxygen slightly diffused into Cu matrix and changed the surface of Cu by forming metal oxide phases. When the processing times were complete at 3 min and 6 min and the system was cooled down, oxides at the surface separated from metal precursors due to the difference of their thermal expansion coefficient. Upon processing at the interval of 9 min, 12 min and 15 min, the particles were reduced in size due to metal oxide formation. In addition, metal oxide particles have dense agglomeration indicating the existence of sintering. The particles were approximately 450 nm in diameter by 15 min processing.

FTIR spectra of various samples are shown in Fig. 6. The as-synthesized samples exhibit absorption bands at approximately 3250–3600 cm^{-1} which can be specified as O—H stretching contributed by water content. The absorption bands at 1383 cm^{-1} was the result of Cu^{2+}—O^{2-} stretching mode peak, which was very close to the report of Li [10] at 1384 cm^{-1}. FTIR spectra detected at 529 cm^{-1} and 585 cm^{-1} can be indexed to the vibrational mode of CuO formation with good corresponding to the result of Padil and Černík [11] at 525 and 580 cm^{-1}. For 1 min processing, a peak appear at 621 cm^{-1} corresponding to Cu(I)—O vibrational mode [12], in accordance with the XRD analysis showing Cu_2O phase in the sample at the same length of operating time.

Photoluminescence (PL) spectrum of the 15 min processed sample was determined at room temperature as shown in Fig. 7. The excitation energy from a Xe arc-lamp at 325 nm wavelength was used. The main emission peak was observed around 402 nm in the violet region. The result is in good agreement with the report of Mukherjee et al. [13], Chang et al. [14] and Maji et al. [15] which have the emission wavelengths at 395 nm, 403 nm and 406 nm, respectively. The reason of the emission is still unclear because a few reports are available on the PL emission spectra of CuO. The previous study of CuO had claimed that the emission peak was caused by the blue shifted emission comparison to the bulk counterpart [13]. The broad shoulder peak shows in the green spectral region corresponding to the study of Chang et al. [14]. According to the above XRD analysis, the samples processed for 1, 3, 6, 9 and 12 min were mixtures of different phases. Thus they are not interesting to be determined the PL emission.

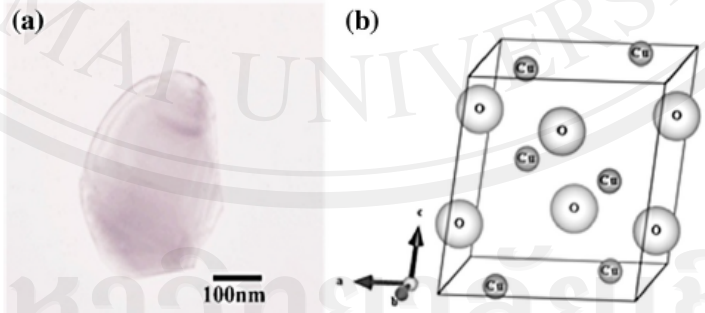

Fig. 4. TEM image of the 15 min as-synthesized CuO sample and its simulated crystal structure.

Please cite this article in press as: A. Klinbumrung, et al., Characterization and gas sensing properties of CuO synthesized by DC directly applying voltage, Appl. Surf. Sci. (2014), http://dx.doi.org/10.1016/j.apsusc.2014.06.037

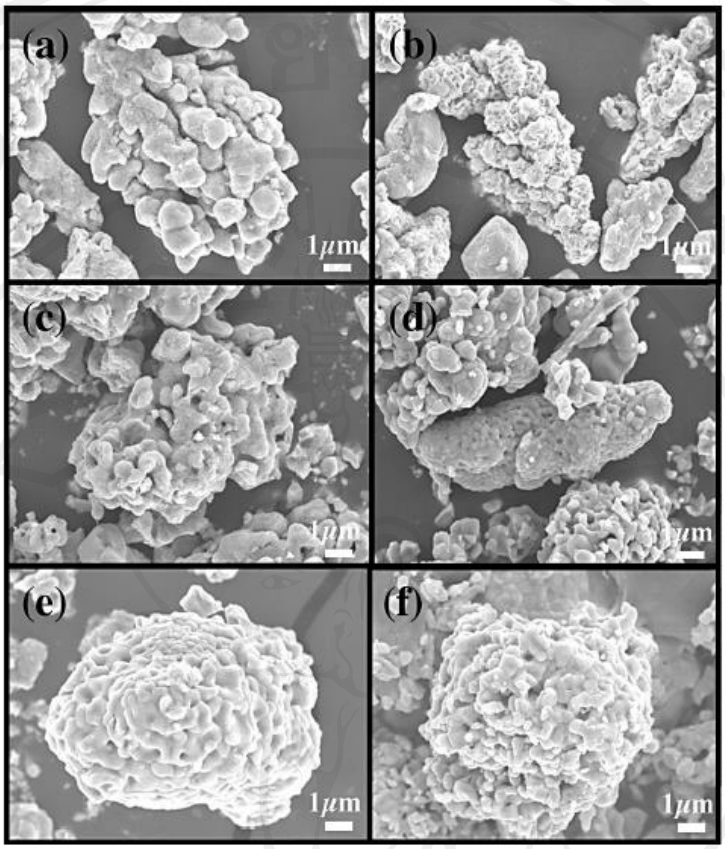

Fig. 5. SEM images of the samples synthesized using different lengths of time ((a)–(f)) 1 min, 3 min, 6 min, 9 min, 12 min and 15 min, respectively.

The surface characterization of the 15 min processed sample was determined by XPS as shown in Fig. 8. The peaks located at 933.8 eV and 953.8 eV are attributed to the Cu $2p_{3/2}$ and Cu $2p_{1/2}$, respectively [16]. The Cu $2p_{3/2}$ peak can be assigned to two Cu–O formation processes (CuO at 933.7 eV and Cu_2O at 932.5 eV) [17]. It is an indicator of the Cu(II) oxidation state. The peaks at 941.7 eV, 944.0 eV and 962.3 eV are assigned to the shakeup lines. The spectrum of O 1s has the range between 527 and 535 eV. The peak at 530.1 eV is related to O^{2-} in CuO and at 531.3 is attributed to oxygen adsorb on the surface of CuO [18]. The intensity of peak at 530.1 eV is stronger than that at 531.3 eV that relied on the adsorbed oxygen rather than O ions in Cu^{2+}–O^{2-} formation. No impurities were detected by the XPS. Thus it reasonably confirms that the as-synthesized sample was CuO.

The theory of inter-band absorption shows that at the fundamental edge the absorption coefficient should vary according to the following equation [19]

$$\alpha h\nu = B(h\nu - E_o)^n, \quad (3)$$

where $h\nu$ is the photon energy in eV, α is the absorption coefficient in cm^{-1}, B is a constant related to the material and the matrix element of the transition, E_0 is the optical energy gap, and n is a pure number which characterizes the transition process: $n = 1/2$ for direct allowed, $n = 2$ for indirect allowed, $n = 3/2$ for direct forbidden, and $n = 3$ for indirect forbidden transitions. The absorption coefficient was calculated using the relation $\alpha d = \ln(1/T)$ where the transmittance T was calculated from the measured absorbance using Beer–Lambert law $A = -\log_{10}(T)$. Here d stands for the path length of the wave in cm and was set equal to the cuvette width of 1 cm.

According to Wood and Tauc equation for photonic absorbance, the energy E_0 can be estimated from the slope and intercept of the linear plot of $(\alpha h\nu)^2$ versus $h\nu$. This dependence is typical of direct allowed transition. From the data of Fig. 9, the energy gap (E_0) is 3.95 eV. This value is close to the report of Kidowaki et al. [20] showing at 3.70 eV and Rehman et al. [5] at 3.72 eV for 20 nm particles. Furthermore, Rehman et al. [5] gave the reason to determine energy gap in direct transition because absorption spectroscopy detecting from indirect transition of CuO by using the UV–vis–NIR is weak.

The electrical characteristics of the 15 min processed CuO deposited as film on alumina substrate has been investigated. The current values of the film were measured by applying voltage interval −20 V to 20 V at various temperatures. The results in the temperature range 200–300 °C operating in air is shown in Fig. 10. The prepared films exhibited straight line characterization that relies on the major mechanism of ohmic current. In the ohmic region, the number of free carriers is higher than the number of applied charge carriers. Thus, free carriers have more influence in

Please cite this article in press as: A. Klinbumrung, et al., Characterization and gas sensing properties of CuO synthesized by DC directly applying voltage, Appl. Surf. Sci. (2014), http://dx.doi.org/10.1016/j.apsusc.2014.06.037

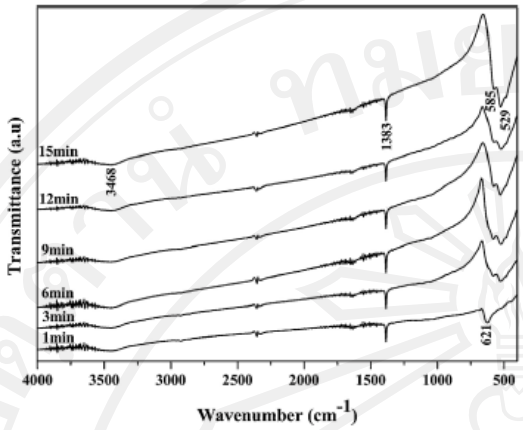

Fig. 6. FTIR spectra of the samples synthesized for 1, 3, 6, 9, 12 and 15 min processing times.

electrical conduction than the electrons which applied to semiconductors. The carrier diffusion in materials both forward and reverse bias is at the same mechanism. Specific contact resistivity (ρ_c) at the temperature of 200, 225, 250, 275 and 300 °C was calculated by the relationship of $\rho_c = V/J$ (J is the current density) which shows the results of 0.142×10^5, 0.057×10^5, 0.037×10^5, 0.020×10^5 and $0.014 \times 10^5\ \Omega\,cm^2$, respectively. The specific contact resistivity was decreased when the temperature was increased because the thermal activation generated more free charge carriers.

The CuO sample processed for15 min was exposed in ammonia–air locked chamber with 1055 ppm concentration of NH_3 gas. The response of the sensor was studied by selecting the operating temperature in the range of 200–300 °C. For the results of Figs. 11 and 12, sensitivity gradually increased when the temperature increased: at 200 °C, 225 °C and 250 °C with the value of 18.5%, 21.0% and 21.9% (highest), respectively. At 250 °C operating temperature, the activating energy could be high enough to form a complete chemical reaction. Further increase of the temperature, more working temperature led to sensitivity decrease with the value of 16.3% at 275 °C and 12.5% at 300 °C because of

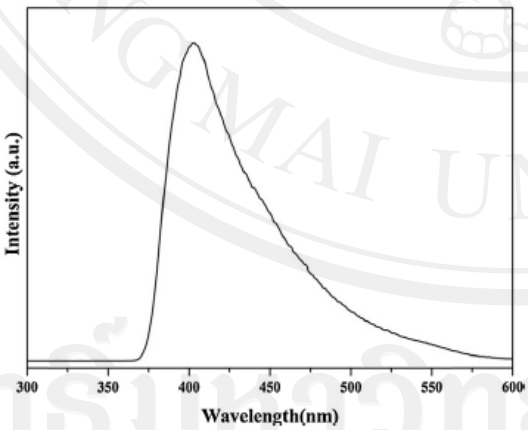

Fig. 7. PL emission of the 15 min as-synthesized CuO sample.

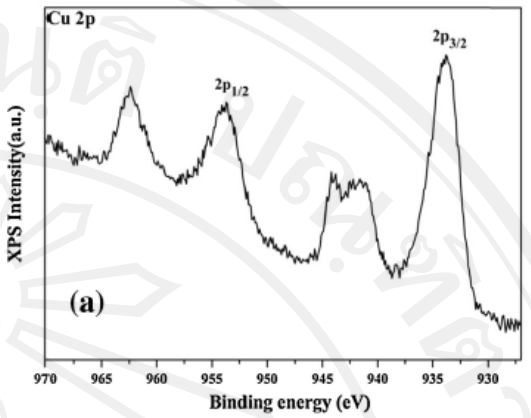

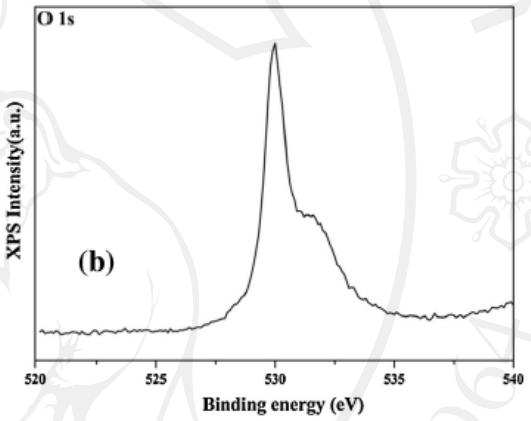

Fig. 8. XPS spectra of the 15 min as-synthesized CuO sample: (a) Cu 2p and (b) O 1s.

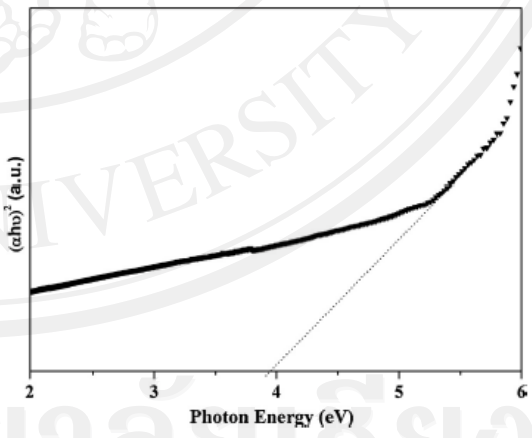

Fig. 9. Direct allowed transition of the 15 min as-synthesized CuO sample.

Please cite this article in press as: A. Klinbumrung, et al., Characterization and gas sensing properties of CuO synthesized by DC directly applying voltage, Appl. Surf. Sci. (2014), http://dx.doi.org/10.1016/j.apsusc.2014.06.037

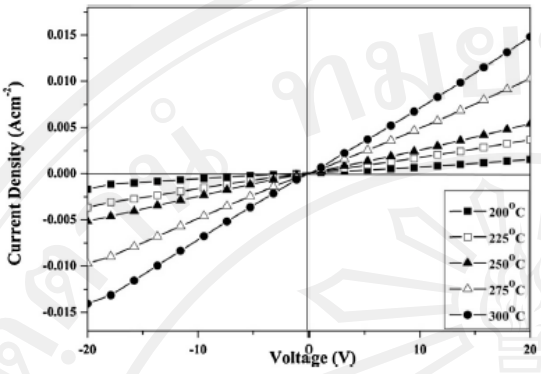

Fig. 10. Symmetric current and voltage performance of the 15 min as-synthesized CuO sample in air at the working temperatures of 200, 225, 250, 275 and 300 °C.

desorption of oxygen ions at the surface. At the initial step while sensor exposing to the tested gas, the sensitivity abruptly increased to the highest value. Then, it went down to reach a new equilibrium point and held at this state. The similar gas sensing behavior was reported by other researchers who studied nanostructured materials to NH_3 gas detection such as copper oxide nanowires [21], tungsten oxide nanowire films [22] and silver nanowires [23]. However, the first increase is unclear. The result could be the cause of distribution of the tested gas with heterogeneous spreading in the closed chamber that made more gas density at some parts and less gas density at others. Static gas testing system spends a time for gas homogeneous distribution.

The current density change of CuO gas sensor to NH_3 in air at various concentrations at 250 °C is shown in Fig. 13. The

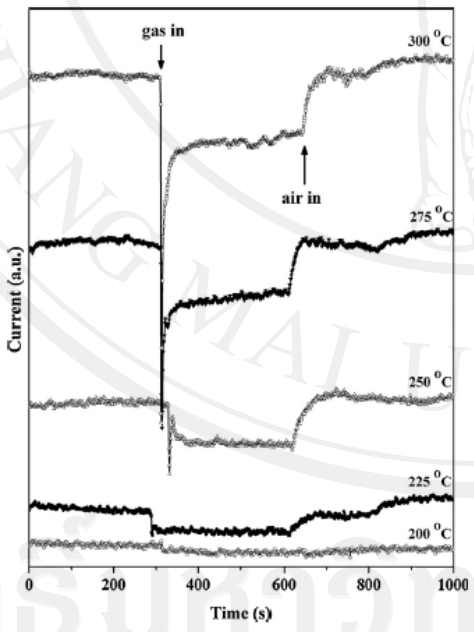

Fig. 11. Dynamic respond-recovery curves of the 15 min as-synthesized CuO sample at the working temperatures of 200, 225, 250, 275 and 300 °C.

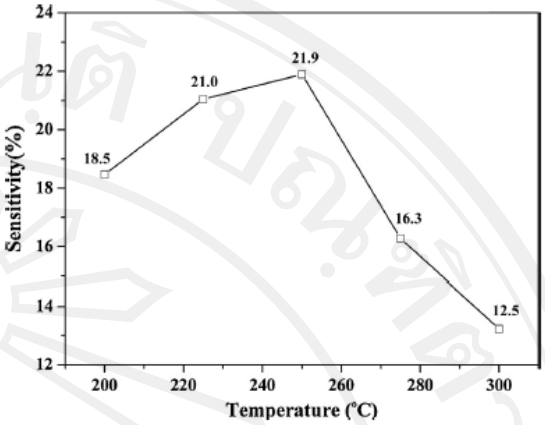

Fig. 12. Sensitivity of the 15 min as-synthesized CuO sample at various working temperatures.

sensitivity of gas sensor as a function of NH_3 concentration is shown in Fig. 14. The linear increase of gas response with concentration increasing was clearly detected. Sensitivity values were found to be 21.9%, 30.2%, 32.1%, 51.0% and 56.6% by exposing to the NH_3–air gas mixture at concentration of 1055, 2110, 3165, 4220 and 5275 ppm of ammonia, respectively. These values were fitted to a linear regression line: $S = 0.00856C + 11.28228$, with C – ammonia concentration. At C – 10,000 ppm, the sensitivity (S) was calculated to be 96.88%. The present sensitivity is very close to the report of Mashock et al. [21]: gas sensing properties of CuO nanowires exposing to 10,000 ppm NH_3 gas concentration at room temperature without surface functionalization have a sensitivity of 92% (evaluated from the $((R_{gas} - R_{air})/R_{air}) \times 100$). The surface of the device can be improved by doping with catalytic nanoparticles.

For the performance of metal oxide gas sensor to the tested gas, the main cause to electrical resistance change is adsorption and desorption of the detected gas at its surface [24]. Oxygen molecules adsorb on CuO at a temperature about 10 °C. These molecules were placed at surface defect sites as electron acceptors. The oxygen ionic species (O_2^-, $O^-$and O^{2-}) originally control by the working temperature, described by the following equations [25].

$$O_2(gas) \leftrightarrow O_2(ads) \quad (4)$$

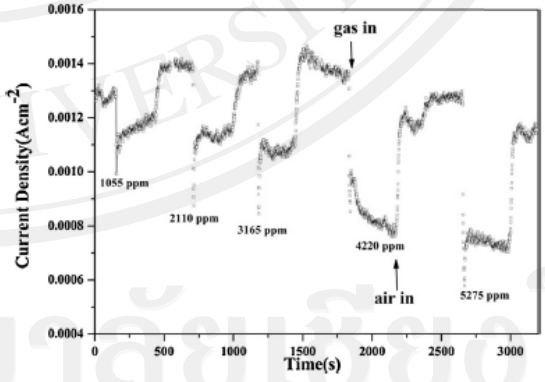

Fig. 13. Current density characteristic of the 15 min as-synthesized CuO sample at different NH_3 concentrations.

Please cite this article in press as: A. Klinbumrung, et al., Characterization and gas sensing properties of CuO synthesized by DC directly applying voltage, Appl. Surf. Sci. (2014), http://dx.doi.org/10.1016/j.apsusc.2014.06.037

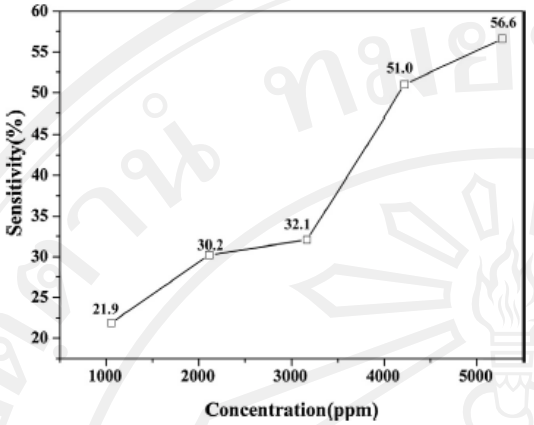

Fig. 14. Sensitivity of the 15 min as-synthesized CuO sample at different NH_3 concentrations.

$$O_2(ads) + e^- \leftrightarrow O_2^-(ads) \quad (5)$$

$$O_2^-(ads) + e^- \leftrightarrow 2O^-(ads) \quad (6)$$

CuO surface was attached by negative charge oxygen ions by the adsorbed and drawn electrons. Thus, holes near the surface increase and influence the increasing conduction as well. When NH_3 gas contaminated on surface, O^- reacted with the tested gas explained by the following equation [26].

$$2NH_3 + 3O^- \rightarrow 3H_2O + N_2 + 3e^- \quad (7)$$

The released electrons went back to valence band. Decreasing the concentration of holes generated the increase of resistance. When the tested gas was replaced by air, the sensor restored to original state.

4. Conclusions

CuO synthesized by 50 A and 3.6 V DC electrical heating method has been successfully synthesized, and was characterized its crystalline structure, morphology, optical properties and gas sensing performance. Monoclinic CuO structure with about 450 nm in diameter showed 3.95 eV energy gap. The PL emission peak is observed at 402 nm wavelength in violet region. The XPS spectrum indicates the Cu(II) oxidation state with the formation of CuO. Gas sensing performance exhibits 21.9% sensitivity to 1055 ppm NH_3 rich at 250 °C working temperature. The as-synthesized CuO can be used as an efficient sensor to ammonia due to its promising advantage for large-scale production with low cost and benign to the environment.

Acknowledgments

We wish to thank the Thailand's Office of the Higher Education Commission for providing financial support through the program of the Higher Education Research Promotion (HERP), and the National Research University (NRU) Project for Chiang Mai University (CMU); and the National Nanotechnology Center (NANOTEC) , National Science and Technology Development Agency (NSTDA), Thailand, for providing financial support through the project P-10-11345, including the Graduate School of CMU through a general support.

References

[1] L.J. Zhou, Y.C. Zou, J. Zhao, P.P. Wang, L.L. Feng, L.W. Sun, D.J. Wang, G.D. Li, Facile synthesis of highly stable and porous Cu_2O/CuO cubes with enhanced gas sensing properties, Sens. Actuators, B: Chem. 188 (2013) 533–539.
[2] M.F. Al-Kuhaili, Characterization of copper oxide thin films deposited by the thermal evaporation of cuprous oxide (Cu_2O), Vacuum 82 (2008) 623–629.
[3] B.J. Hansen, G. Lu, J. Chen, Direct oxidation growth of CuO nanowires from copper-containing substrates, J. Nanomater. 2008 (2008) 7, Art. ID830474.
[4] A.P. Moura, L.S. Cavalcante, J.C. Sczancoski, D.G. Stroppa, E.C. Paris, A.J. Ramirez, J.A. Varela, E. Longo, Structure and growth mechanism of CuO plates obtained by microwave-hydrothermal without surfactants, Adv. Powder Technol. 21 (2010) 197–202.
[5] S. Rehman, A. Mumtaz, S.K. Hasanain, Size effects on the magnetic and optical properties of CuO nanoparticles, J. Nanopart. Res. 13 (2011) 2497–2507.
[6] A. El-Trass, H. ElShamy, I. El-Mehasseb, M. El-Kemary, CuO nanoparticles: synthesis, characterization, optical properties and interaction with amino acids, Appl. Surf. Sci. 258 (2012) 2997–3001.
[7] T.J.B. Holland, S.A.T. Redfern, Unit cell refinement from powder diffraction data: the use of regression diagnostics, Mineral. Mag. 61 (1997) 65–77.
[8] M.R. Johan, M.S.M. Suan, N.L. Hawari, H.A. Ching, Annealing effects on the properties of copper oxide thin films prepared by chemical deposition, Int. J. Electrochem. Sci. 6 (2011) 6094–6104.
[9] M.T.S. Nair, L. Guerrero, O.L. Arenas, P.K. Nair, Chemically deposited copper oxide thin films: structural, optical and electrical characteristics, Appl. Surf. Sci. 150 (1999) 143–151.
[10] Y. Li, Synthesis of copper(II) oxide particle and detection of photoelectrochemically generated hydrogen, in: 2008 NNIN REU Research Accomplishments, NNIN, 2008, pp. 46–47.
[11] V. Vellora, T. Padil, M. Černík, Green synthesis of copper oxide nanoparticles using gum karaya as a biotemplate and their antibacterial application, Int. J. Nanomed. 8 (2013) 889–898.
[12] V. Andal, G. Buvaneswari, Preparation of Cu_2O nano-colloid and its application as selective colorimetric sensor for Ag^+ ion, Sens. Actuators Chem. B155 (2011) 653–658.
[13] N. Mukherjee, B. Show, S.K. Maji, U. Madhu, S.K. Bhar, B.C. Mitra, G.G. Khan, A. Mondal, CuO nano-whiskers: electrodeposition, Raman analysis, photoluminescence study and photocatalytic activity, Mater. Lett. 65 (2011) 3248–3250.
[14] S.S. Chang, H.J. Lee, H.J. Park, Photoluminescence properties of spark-processed CuO, Ceram. Int. 31 (2005) 411–415.
[15] S.K. Maji, N. Mukherjee, A. Mondal, B. Adhikary, B. Karmakar, Chemical synthesis of mesoporous CuO from a single precursor: structural, optical and electrical properties, J. Solid State Chem. 183 (2010) 1900–1904.
[16] R.A. Zarate, F. Hevia, S. Fuentes, V.M. Fuenzalida, A. Zúñiga, Novel route to synthesize CuO nanoplatelets, J. Solid State Chem. 180 (2007) 1464–1469.
[17] J.F. Moulder, W.F. Stickle, P.E. Sobol, K.D. Bomben, Handbook of X-ray Photoelectron Spectros, Perkin-Elmer, Eden Prairie, MN, 1992.
[18] D.I. Son, C.H. You, T.W. Kim, Structural, optical, and electronic properties of colloidal CuO nanoparticles formed by using a colloid-thermal synthesis process, Appl. Surf. Sci. 255 (2009) 8794–8797.
[19] G. Burns, Solid State Physics, Academic Press, New York, NY, 1985.
[20] H. Kidowaki, T. Oku, T. Akiyama, A. Suzuki, B. Jeyadevan, J. Cuya, Fabrication and characterization of CuO-based solar cells, J. Mater. Sci. Res. 1 (2012) 138–143.
[21] M. Mashock, K. Yu, S. Cui, S. Mao, G. Lu, J. Chen, Modulating gas sensing properties of CuO nanowires through creation of discrete nanosized *p–n* junctions on their surfaces, Appl. Mater. Interfaces 4 (2012) 4192–4199.
[22] Y.M. Zhao, Y.Q. Zhu, Room temperature ammonia sensing properties of $W_{18}O_{49}$ nanowires, Sens. Actuators Chem. B137 (2009) 27–31.
[23] W. Xing, J. Hu, S.C. Kung, K.C. Donavan, W. Yan, R. Wu, R.M. Penner, A chemically-responsive nanojunction within a silver nanowire, Nano Lett. 12 (2012) 1729–1735.
[24] N. Barsan, C. Simion, T. Heine, S. Pokhrel, U. Weimar, Modeling of sensing and transduction for p-type semiconducting metal oxide based gas sensors, J. Electroceram. 25 (2010) 11–19.
[25] T.T. Trinh, N.H. Tu, H.H. Le, K.Y. Ryu, K.B. Le, K. Pillai, J. Yi, Improving the ethanol sensing of ZnO nano-particle thin films—the correlation between the grain size and the sensing mechanism, Sens. Actuators, B: Chem. 152 (2011) 73–81.
[26] M.S. Wagh, G.H. Jain, D.R. Patil, S.A. Patil, L.A. Patil, Modified zinc oxide thick film resistors as NH_3 gas sensor, Sens. Actuators, B: Chem. 115 (2006) 128–133.

Please cite this article in press as: A. Klinbumrung, et al., Characterization and gas sensing properties of CuO synthesized by DC directly applying voltage, Appl. Surf. Sci. (2014), http://dx.doi.org/10.1016/j.apsusc.2014.06.037